Engineering Fracture Mechanics, **41**, 203–221 (1992).

The Formation and Effect of Outer-Ply Microcracks in Cross-Ply Laminates: A Variational Approach

John A. Nairn and Shoufeng Hu

Department of Materials Science and Engineering,

University of Utah, Salt Lake City, Utah 84112, USA

ABSTRACT

The microcracking process in laminates which have outer-ply 90° plies (e.g. $[90_m/0_n]_s$) has some important differences from the microcracking process in laminates which lack outer-ply 90° plies (e.g. $[0_n/90_m]_s$). Foremost among the differences is the characteristic damage state. $[90_m/0_n]_s$ laminates form antisymmetric or staggered microcracks while $[0_n/90_m]_s$ laminates form symmetric microcracks. To explain observed differences, this paper presents a variational mechanics analysis of the stresses and the energy release rate in a $[90_m/0_n]_s$ laminate having staggered microcracks. The new analysis and a previous analysis of $[0_m/90_n]_s$ laminates are used to assess the effect of laminate structure on the mechanical properties and failure properties of cross-ply laminates. The findings are: 1. A given level of microcracking damage causes a greater amount of degradation in mechanical properties in $[90_m/0_n]_s$ laminates than in the corresponding $[0_n/90_m]_s$ laminates. 2. Although $[90_m/0_n]_s$ laminates will initiate microcracks at lower loads, the corresponding $[0_n/90_m]_s$ laminates will develop more microcracks after continued loading. 3. A bending effect present in $[90_m/0_n]_s$ laminates but not in $[0_n/90_m]_s$ laminates promotes mode I delamination in $[90_m/0_n]_s$ laminates.

INTRODUCTION

The initial form of damage in cross-ply laminates loaded in tension is transverse matrix cracking or microcracking in the 90° plies (e.g. [1–8]). Microcracks are observed during static tensile loading [1–8], fatigue loading [3,9,10], or thermal loading [11,12]. The study of microcracks has commonly been done using experiments on cross-ply laminates of generic layup $[0_n/90_m]_s$ [1–13]. These laminates have a 90° ply group in the middle. Their characteristic damage state is a roughly periodic array of microcracks with each microcrack spanning the entire cross-section of the 90° ply group [3,13].

An important class of cross-ply laminates that has received significantly less study is laminates of generic layup $[90_m/0_n]_s$ or laminates which have outer-ply 90° ply groups. The characteristic damage state of $[90_m/0_n]_s$ laminates is again a roughly periodic array of microcracks in each of the two 90° ply groups with each microcrack spanning the entire cross-section of its' ply group [3,13,14]. Unlike $[0_n/90_m]_s$ laminates, however, $[90_m/0_n]_s$ laminates have two 90° ply groups and the description of the characteristic damage state must include a description of the relation between the microcracks in one 90°ply group and those in the other 90° ply group. The few observations available [3,14] show that if the microcrack density is high enough, the

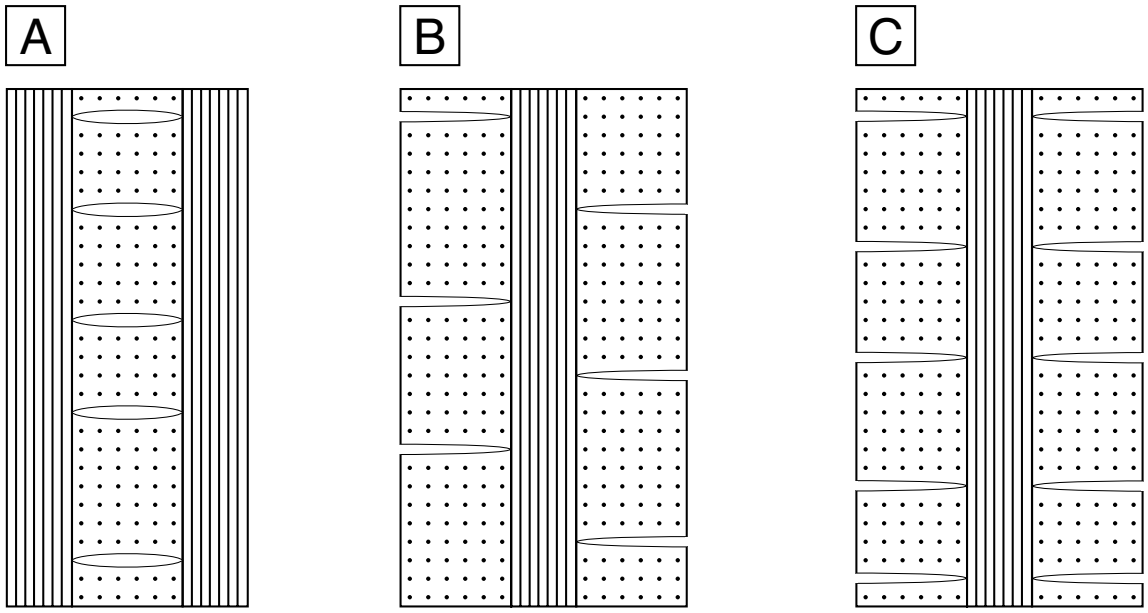

Figure 1: The characteristic damage state of A: $[0_n/90_m]_s$ laminate, B: $[90_m/0_n]_s$ laminate having "staggered" or antisymmetric microcracks, C: $[90_m/0_n]_s$ laminate having symmetric microcracks (this symmetric damage state is sometimes assumed in analyses but is never observed in experiments.)

cracks in the two 90° ply groups are "staggered." By staggered microcracks we mean that the microcracks in one 90° ply group are shifted by half a crack interval from the microcracks in the other 90° ply group. Figure 1 shows the characteristic damage states of $[0_n/90_m]_s$ and $[90_m/0_n]_s$ laminates. Also shown in Fig. 1 is a "nonstaggered" characteristic damage state in $[90_m/0_n]_s$ laminates. The nonstaggered damage state is included for comparison and because it is the damage state assumed in some analyses [15–17]. To our knowledge, the nonstaggered characteristic damage state is never observed in $[90_m/0_n]_s$ laminates during experiments.

Besides the differences in the characteristic damage state, there are other significant differences between microcracking in $[0_n/90_m]_s$ and in $[90_m/0_n]_s$ laminates. The crack density as a function of applied load is layup dependent. In particular, the applied stress to cause the initial microcrack and the saturation crack density are both functions of the stacking sequence. In $[90_m/0_n]_s$ laminates, these quantities are both lower than the corresponding quantities in $[0_n/90_m]_s$ laminates [3,13]. Highsmith and Reifsnider [3] report the stiffness reduction due to microcracks in outer-ply 90° ply groups. The stiffness reduction differs, in details, from the stiffness reduction of the corresponding $[0_n/90_m]_s$ laminate. Hashin [16] has analyzed the effect of inner- and outer-ply cracks on the thermal expansion coefficient; the calculated effects are different.

The differences between the microcracking properties of $[90_m/0_n]_s$ and $[0_n/90_m]_s$ laminates described above suggest that more analyses and experiments on $[90_m/0_n]_s$ laminates aimed at explaining those differences would be desirable. Explaining those differences has more significance than "academic" interest. All cross-ply laminates have outer-ply 90° ply groups when viewed from some particular direction. $[0_n/90_m]_s$ laminates, for example, when viewed from the transverse direction are seen as $[90_n/0_m]_s$ laminates. Due to this bidirectional nature of cross-ply laminates, any cross-ply laminate subjected to biaxial loading, or to

transverse loading in the case of $[0_n/90_m]_s$ laminates, will be prone to the development of microcracks in outer-ply 90° ply groups. One important biaxial loading example is thermal loading. Due to a mismatch in the thermal expansion coefficients of 0° and 90° plies, any cross-ply laminate subjected to thermal cycling will experience biaxial thermal loading. Thermal loading of $[0_m/90_n]_s$ laminates has been observed to cause microcracks in both inner and outer plies [12].

Analyses of $[0_n/90_m]_s$ laminates can be classified as "shear-lag" analysis when they are based on shear-lag assumptions or when they reduce to results that are equivalent to those based on shear-lag assumptions (e.g. [2,4,6,7,18,19]). All these analyses are one-dimensional or at best quasi-two-dimensional [e.g. 19]. Because a one-dimensional analysis does not include transverse stresses, it makes no distinction between $[0_n/90_m]_s$ and $[90_m/0_n]_s$ laminates and these one-dimensional analyses of $[0_n/90_m]_s$ are, by default, also analyses of $[90_m/0_n]_s$ laminates. Because the resulting solutions are identical, however, such analyses are of no help in explaining the observed differences between $[0_n/90_m]_s$ and $[90_m/0_n]_s$ laminates. Explanation of the observed differences can only come from an accurate two-dimensional analysis. The most promising approach appears to be the variational mechanics approach originally developed by Hashin [20,21,22]. This type of analysis was shown to accurately predict the stiffness reduction of $[0_n/90_m]_s$ laminates [20]. It has subsequently been extended and used to explain the microcracking fracture and fatigue behavior of $[0_n/90_m]_s$ laminates [15,23,24].

This paper presents a new variational mechanics analysis of $[90_m/0_n]_s$ laminates. An important aspect of this new analysis is that it accounts for antisymmetric or staggered microcracks. The occurrence of staggered microcracks *vs.* nonstaggered microcracks adds significant complication to the analysis. Is the extra complication necessary? In extending Hashin's [20,21] analysis to fracture problems, Nairn [15] included an analysis of $[90_m/0_n]_s$ laminates with nonstaggered microcracks (see Fig. 1C) as a trivial extension of a $[0_n/90_m]_s$ analysis. Recent experimental results [14], however, show that for $[90_m/0_n]_s$ laminates with staggered microcracks, the nonstaggered microcrack analysis is not in good agreement with experimental results. We thus conclude that previous analyses that have resorted to the simplified assumption of nonstaggered outer-ply microcracks [e.g. 15,16,17,22] may not provide quantitatively accurate predictions. The analysis in this paper is the first to account for the observed existence of staggered microcracks in $[90_m/0_n]_s$ laminates.

AN ADMISSIBLE STRESS STATE

Consider an n-layer multilayered sample under a uniaxial stress σ_0 in the x direction (see Fig. 2A) and at the thermal stress-free temperature T_0. When there is no damage, each layer will be under a state of uniform, uniaxial stress:

$$\sigma_{xx}^{(i)} = \sigma_{x0}^{(i)} = k^{(i)}\sigma_0 = \frac{E_x^{(i)}}{E_0}\sigma_0 \tag{1}$$

$$\sigma_{xz}^{(i)} = \sigma_{zz}^{(i)} = 0 \tag{2}$$

In this notation, superscript (i) refers to a stress or property in layer i, k is an effective stiffness, E_x is the x-direction Young's modulus, and E_0 is the x-direction Young's modulus of the undamaged laminate. The last equality in Eq. (1) follows from an assumption of constant x-direction axial strain in the undamaged

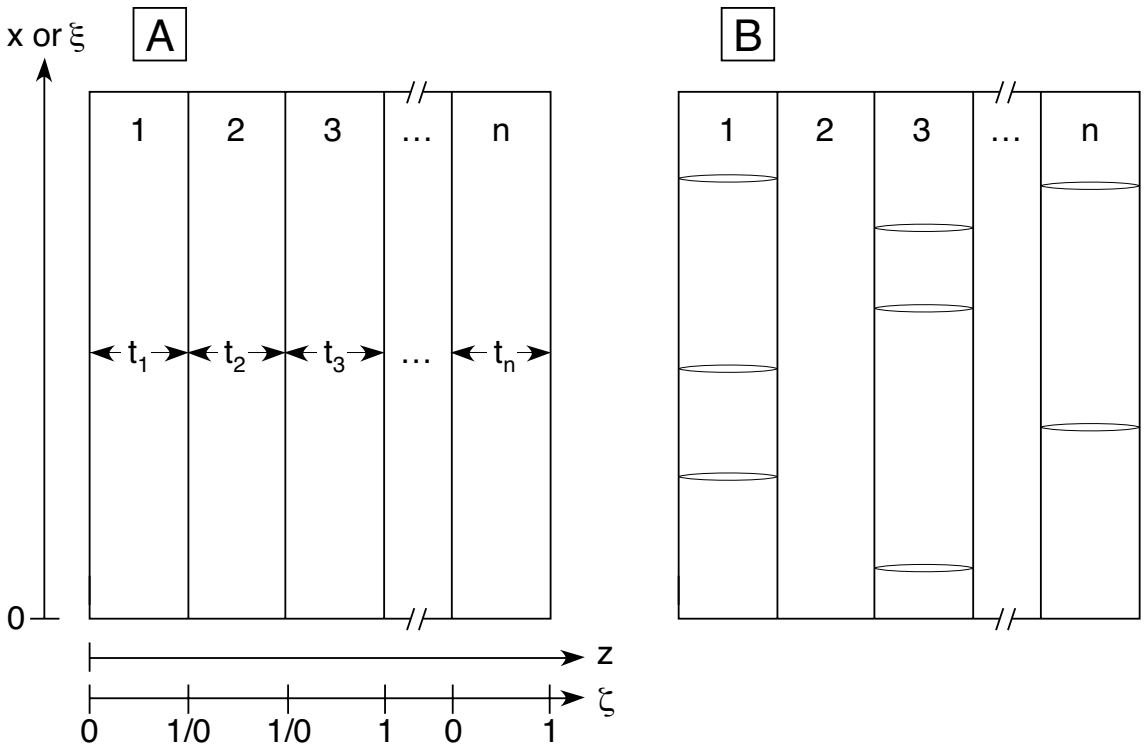

Figure 2: An n layer multilayered structure showing the coordinate system and some of the terms defined in this paper. A: An undamaged multilayered structure. B: The same multilayered structure after damage.

sample. We next impose an arbitrary state of damage on the n-layer multilayered sample (see Fig. 2B). The damage will be caused by an increase in load and/or a change in temperature to T_s. The presence of damage will perturb the stresses in each layer. Following Hashin [20,21] we make one and only one assumption—that the new x-axis tensile stresses ($\sigma_{xx}^{(i)}$) are independent of the z-axis or transverse direction within each layer. A general stress state that fulfills this assumption and simultaneously satisfies stress equilibrium can easily be derived as:

$$\sigma_{xx}^{(i)} = \sigma_{x0}^{(i)} - \psi_i \tag{3}$$

$$\sigma_{xz}^{(i)} = \lambda_i F_i \tag{4}$$

$$\sigma_{zz}^{(i)} = -\lambda_i^2 f_i \tag{5}$$

where $\lambda_i = \frac{t_i}{t_1}$, t_i is the thickness of the i^{th} layer, $\psi_i(\xi)$ is a function of the dimensionless x-direction coordinate ξ ($\xi = x/t_1$), and $F_i(\xi,\zeta)$ and $f_i(\xi,\zeta)$ are functions of ξ and of the dimensionless z-direction coordinate ζ:

$$\zeta = \frac{z - \sum_{j=1}^{i-1} t_j}{t_i} \tag{6}$$

which runs from 0 to 1 within each layer. The functions F_i, f_i, and ψ_i are interrelated by equilibrium:

$$\frac{\partial F_i}{\partial \xi} = \frac{\partial f_i}{\partial \zeta} \tag{7}$$

$$\psi_i' = \frac{d\psi_i}{d\xi} = \frac{\partial F_i}{\partial \zeta} \tag{8}$$

Integrating these expressions, the functions F_i and f_i have the general form

$$F_i = \psi_i'(\xi)\zeta + g_i(\xi) \tag{9}$$

$$f_i = \frac{1}{2}\psi_i''(\xi)\zeta^2 + g_i'(\xi)\zeta + h_i(\xi) \tag{10}$$

where $g_i(\xi)$ and $h_i(\xi)$ are two arbitrary functions of ξ.

That the above stress state satisfies equilibrium can be verified by substituting it into the stress equilibrium equations. To be an admissible stress state, the stresses must further satisfy traction boundary conditions and continuity conditions for shear and transverse stresses between layers. First, the stress-free surfaces at the start of layer 1 and at the end of layer n imply that $\sigma_{xz}^{(1)}(0) = \sigma_{zz}^{(1)}(0) = 0$ and $\sigma_{xz}^{(n)}(1) = \sigma_{zz}^{(n)}(1) = 0$. With these boundary conditions and Eqs. (9) and (10) we find

$$\begin{aligned} F_1 &= \psi_1'\zeta & f_1 &= \frac{1}{2}\psi_1''\zeta^2 \\ F_n &= \psi_n'(\zeta - 1) & f_n &= \frac{1}{2}\psi_n''(\zeta - 1)^2 \end{aligned} \tag{11}$$

If we know F_i and f_i in layer i we can derive F_{i+1} and f_{i+1} (for $i \neq n$) using the stress continuity conditions $\sigma_{xz}^{(i)}(1) = \sigma_{xz}^{(i+1)}(0)$ and $\sigma_{zz}^{(i)}(1) = \sigma_{zz}^{(i+1)}(0)$. Likewise we can derive F_{i-1} and f_{i-1} (for $i \neq 1$) using the stress continuity conditions $\sigma_{xz}^{(i)}(0) = \sigma_{xz}^{(i-1)}(1)$ and $\sigma_{zz}^{(i)}(0) = \sigma_{zz}^{(i-1)}(1)$. The results are

$$F_{i+1} = \psi_{i+1}'\zeta + \frac{\lambda_i F_i(\xi, 1)}{\lambda_{i+1}} \tag{12}$$

$$f_{i+1} = \frac{1}{2}\psi_{i+1}''\zeta^2 + \frac{\lambda_i\zeta}{\lambda_{i+1}}\frac{\partial F_i(\xi, 1)}{\partial\xi} + \frac{\lambda_i^2 f_i(\xi, 1)}{\lambda_{i+1}^2} \tag{13}$$

$$F_{i-1} = \psi_{i-1}'(\zeta - 1) + \frac{\lambda_i F_i(\xi, 0)}{\lambda_{i-1}} \tag{14}$$

$$f_{i-1} = \frac{1}{2}\psi_{i-1}''(\zeta - 1)^2 + \frac{\lambda_i(\zeta - 1)}{\lambda_{i-1}}\frac{\partial F_i(\xi, 0)}{\partial\xi} + \frac{\lambda_i^2 f_i(\xi, 0)}{\lambda_{i-1}^2} \tag{15}$$

Having established F_1, f_1, F_n, and f_n, F_i and f_i for all i can be found from Eqs. (12)–(15) by induction.

From the general results that began this section we derive a specific result for the stress state in a $[90_m/0_n]_s$ laminate in the presence of staggered microcracks. A four-layer unit cell of damage is show in Fig. 3A. Layers 1 and 4 are 90° ply groups. Layers 2 and 3 split the 0° ply group into two layers. The unit cell of damage extends from $x = -a$ to $x = +a$ or from $\xi = -\rho$ to $\xi = +\rho$ where $\rho = a/t_1$. Layer 1 has microcracks located at $\xi = \pm\rho$. Due to crack stagger, the microcrack in layer 4 is located at $\xi = 0$. Unlike $[0_n/90_m]_s$ laminates or $[90_m/0_n]_s$ laminates with the simplified assumption of nonstaggered microcracks (see Fig. 1C), the $[90_m/0_n]_s$ laminate with staggered microcracks is no longer symmetric about the midplane (the plane between layers 2 and 3). Although previous analyses for symmetric problems only needed to consider half the laminate or two of the layers [15,20,21], our new analysis which accounts for staggered microcracks must consider all four layers. In short, the antisymmetric damage state complicates the stress analysis.

Although the damage state is not symmetric about the midplane, the ply dimensions and mechanical properties are symmetric about the midplane. We thus have $t_3 = t_2$, $t_4 = t_1$, $\lambda_4 = \lambda_1 = 1$ and $\lambda_3 = \lambda_2 =$

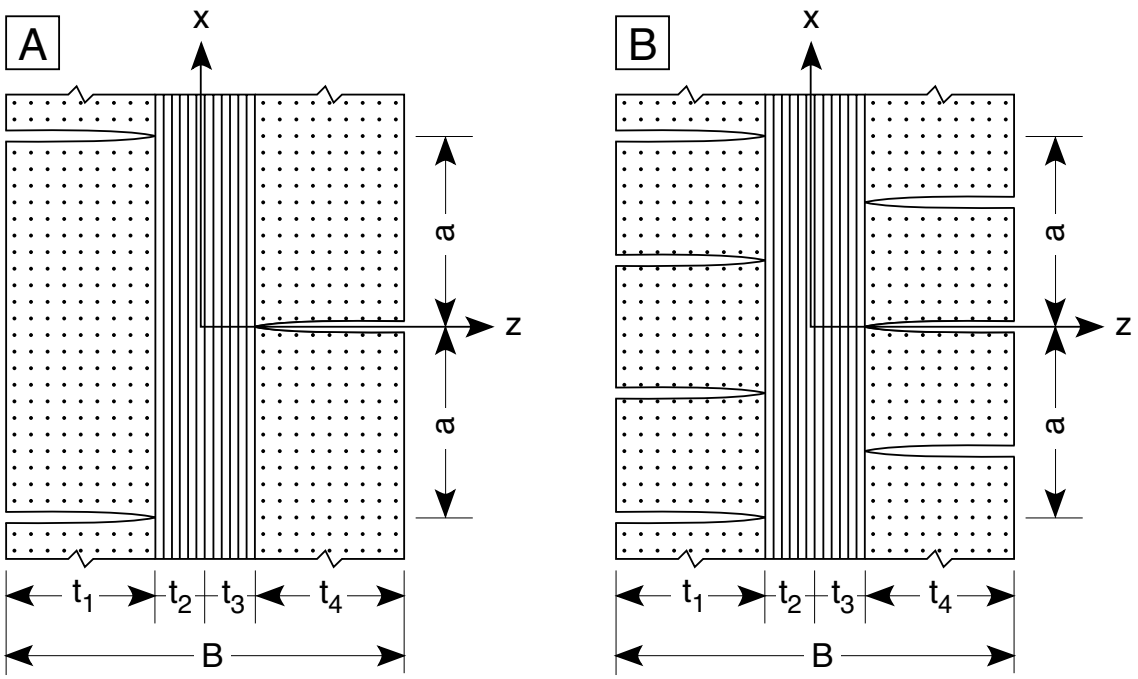

Figure 3: A unit cell of damage in an $[90_m/0_n]_s$ having "staggered" or antisymmetric microcracks. A: A single unit cell of damage. B: Three unit cells of damage after formation of new microcracks at locations of local maxima in tensile stress.

$\lambda = t_2/t_1$. Using these relations and setting $n = 4$ yields

$$\begin{aligned} F_1 &= \psi_1'\zeta & f_1 &= \frac{1}{2}\psi_1''\zeta^2 \\ F_2 &= \psi_2'\zeta + \frac{1}{\lambda}\psi_1' & f_2 &= \frac{1}{2}\psi_2''\zeta^2 + \frac{1}{\lambda}\psi_1''\zeta + \frac{1}{2\lambda^2}\psi_1'' \\ F_3 &= \psi_3'(\zeta-1) - \frac{1}{\lambda}\psi_4' & f_3 &= \frac{1}{2}\psi_3''(\zeta-1)^2 - \frac{1}{\lambda}\psi_4''(\zeta-1) + \frac{1}{2\lambda^2}\psi_4'' \\ F_4 &= \psi_4'(\zeta-1) & f_4 &= \frac{1}{2}\psi_4''(\zeta-1)^2 \end{aligned} \tag{16}$$

where F_2 and f_2 were derived using Eqs. (12) and (13) and F_3 and f_3 were derived using Eqs. (14) and (15).

The stress state in Eq. (16) depends on four functions of ξ—ψ_1, ψ_2, ψ_3, and ψ_4. We can eliminate two of these functions using force balance and stress continuity conditions between layers 2 and 3. By force balance

$$\sum_{i=1}^{4} t_i \sigma_{xx}^{(i)} = \sum_{i=1}^{4} t_i \sigma_{x0}^{(i)} \tag{17}$$

which reduces to

$$\lambda(\psi_2 + \psi_3) = -\psi_1 - \psi_4 \tag{18}$$

Transverse stress continuity between layers 2 and 3 implies that $\sigma_{xx}^{(2)}(1) = \sigma_{xx}^{(3)}(0)$, which eventually yields

$$-\lambda^2(\psi_2 - \psi_3) = (1 + 2\lambda)(\psi_1 - \psi_4) \tag{19}$$

Shear stress continuity between layers 2 and 3 implies that $\sigma_{xz}^{(2)}(1) = \sigma_{xz}^{(3)}(0)$. This condition reduces to the first derivative of Eq. (18) and thus provides no additional constraint. Differentiating Eq. (18) twice and

simultaneously solving the resultant equation and Eq. (19) for ψ_2'' and ψ_3'' yields

$$\psi_2'' = A\psi_1'' + B\psi_4'' \tag{20}$$

$$\psi_3'' = B\psi_1'' + A\psi_1'' \tag{21}$$

where

$$A = -\frac{1+3\lambda}{2\lambda^2} \qquad B = \frac{1+\lambda}{2\lambda^2} \tag{22}$$

Because the unit cell of damage is symmetric about a plane through $\xi = 0$, ψ_i must be an even function and ψ_i' must be an odd function. Using these symmetry conditions, we can integrate Eqs. (20) and (21) to get

$$\psi_2' = A\psi_1' + B\psi_4' \tag{23}$$

$$\psi_3' = B\psi_1' + A\psi_4' \tag{24}$$

The integration constant must be zero to preserve the odd symmetry of ψ_i'. Integrating Eqs. (20) and (21) a second time and using force balance yield

$$\psi_2 = A\psi_1 + B\psi_4 + \eta \tag{25}$$

$$\psi_3 = B\psi_1 + A\psi_4 - \eta \tag{26}$$

where η is an integration constant. We argue that far away from any cracks, the functions ψ_1 to ψ_4 must simultaneously approach zero. For this behavior to occur η must be zero and thus

$$\psi_2 = A\psi_1 + B\psi_4 \tag{27}$$

$$\psi_3 = B\psi_1 + A\psi_4 \tag{28}$$

COMPLEMENTARY ENERGY MINIMIZATION

The equations in the previous section define an admissible stress state for a $[90_m/0_n]_s$ laminate damaged with staggered microcracks. The stress state obeys equilibrium, all traction boundary conditions, and stress continuity between layers. The stress state is expressed in terms of two unknown functions of ξ — ψ_1 and ψ_4. By the principle of minimum complementary energy, the functions ψ_1 and ψ_4 that produce the minimum complementary energy will provide the best approximation to the stress state in a microcracked laminate. For thermoelastic analyses, a variational solution that minimizes complementary energy is found by minimizing the functional Γ given by

$$\Gamma = \frac{1}{2}\int_V \vec{\sigma}\cdot\mathbf{K}\vec{\sigma}dV + \int_V \vec{\sigma}\cdot\vec{\alpha}TdS - \int_{S_1}\vec{\sigma}\cdot\hat{u}dS \tag{29}$$

where $\vec{\sigma}$ is the stress tensor, $\mathbf{K}$ is the compliance tensor, $\vec{\alpha}$ is the thermal expansion coefficient tensor, $T = T_s - T_0$ is the difference between the sample temperature (T_s) and the stress-free temperature (T_0), V is the volume of the laminate, and S_1 is that part of the laminate surface subjected to a fixed displacement

[25]. In this problem S_1 is null. Note that for the two dimensional analysis described in this paper the stress and thermal expansion coefficient tensors are written as vectors: $\vec{\sigma} = (\sigma_{xx}, \sigma_{zz}, \sigma_{xz})$ and $\vec{\alpha} = (\alpha_x, \alpha_z, \alpha_{xz})$.

Substituting the $[90_m/0_n]_s$ laminate stress state into Eq. (29) and assuming that each ply group is orthotropic with at least one of the material axes coincident with either the x or z axis, Γ per unit depth for the region $-a < x < a$ (or $-\rho < \xi < \rho$) is

$$\Gamma = \Gamma_0 + t_1^2 \sum_{i=1}^{4} \int_{-\rho}^{\rho} \left[\frac{\lambda_i \psi_i^2}{2E_x^{(i)}} - \frac{\nu_{xz}^{(i)} \lambda_i^3 \psi_i}{E_x^{(i)}} \int_0^1 f_i d\zeta + \frac{\lambda_i^5}{2E_z^{(i)}} \int_0^1 f_i^2 d\zeta + \frac{\lambda_i^3}{2G_{xz}^{(i)}} \int_0^1 F_i^2 d\zeta \right. \\ \left. + \lambda_i^3 \left(\frac{\sigma_{x0}^{(i)} \nu_{xz}^{(i)}}{E_x^{(i)}} - \alpha_z^{(i)} T \right) \int_0^1 f_i d\zeta - \alpha_x^{(i)} \lambda_i T \psi_i \right] d\xi \tag{30}$$

where $E_x^{(i)}$, $E_z^{(i)}$, $G_{xz}^{(i)}$, $\nu_{xz}^{(i)}$, $\alpha_x^{(i)}$, and $\alpha_z^{(i)}$ are the mechanical and thermal expansion properties of the i^{th} layer, being, respectively, x and z direction Young's moduli, in-plane shear modulus, in-plane Poisson's ratio, and x and z direction thermal expansion coefficients. The term Γ_0 is a constant energy term that does not enter energy minimization procedures:

$$\Gamma_0 = 2\rho t_1^2 \sum_{i=1}^{4} \lambda_i \left(\frac{{\sigma_{x0}^{(i)}}^2}{2E_x^{(i)}} + \alpha_x^{(i)} T \sigma_{x0}^{(i)} \right) \tag{31}$$

Substituting the expressions for F_i, f_i, ψ_2 and ψ_3 into Eq. (30) and evaluating all the ζ integrals (which can be evaluated in closed form) result in

$$\Gamma - \Gamma_0 = t_1^2 \int_{-\rho}^{\rho} \Big(C_{11}(\psi_1^2 + \psi_4^2) + C_{21}(\psi_1 \psi_1'' + \psi_4 \psi_4'') + C_{31}(\psi_1''^2 + \psi_4''^2) + C_{41}(\psi_1'^2 + \psi_4'^2) \\ - \Delta\alpha T(\psi_1 + \psi_4) + C_{12}\psi_1\psi_4 + C_{22}(\psi_1\psi_4'' + \psi_1''\psi_4) + C_{32}\psi_1''\psi_4'' + C_{42}\psi_1'\psi_4' \Big) d\xi \tag{32}$$

where $\Delta\alpha = \alpha_x^{(1)} - \alpha_x^{(2)}$ and C_{ij} are constants that depend on the dimensions and mechanical properties of the layers:

$$C_{11} = \frac{1}{2E_x^{(1)}} + \frac{\lambda}{2E_x^{(2)}}(A^2 + B^2) \tag{33}$$

$$C_{21} = -\frac{1}{6}\left(\frac{\nu_{xz}^{(1)}}{E_x^{(1)}} + \frac{\nu_{xz}^{(2)} \lambda^3}{E_x^{(2)}} \left(A^2 + B^2 + \frac{3A}{\lambda} + \frac{3A}{\lambda^2} \right) \right) \tag{34}$$

$$C_{31} = \frac{1}{120}\left(\frac{3}{E_z^{(1)}} + \frac{\lambda}{E_z^{(2)}} \left(3(A^2 + B^2)\lambda^4 + 15A\lambda^3 + 10(A+2)\lambda^2 + 30\lambda + 15 \right) \right) \tag{35}$$

$$C_{41} = \frac{1}{6G_{xz}^{(1)}} + \frac{\lambda^3}{2G_{xz}^{(2)}} \left(\frac{A^2 + B^2}{3} + \frac{A}{\lambda} + \frac{1}{\lambda^2} \right) \tag{36}$$

$$C_{12} = \frac{2\lambda AB}{E_x^{(2)}} \tag{37}$$

$$C_{22} = -\frac{1}{6}\left(\frac{\nu_{xz}^{(2)} \lambda^3}{E_x^{(2)}} \left(2AB + \frac{3B}{\lambda} + \frac{3B}{\lambda^2} \right) \right) \tag{38}$$

$$C_{32} = \frac{\lambda}{60E_z^{(2)}} \left(6AB\lambda^4 + 15B\lambda^3 + 10B\lambda^2 \right) \tag{39}$$

$$C_{42} = \frac{\lambda^3}{G_{xz}^{(2)}} \left(\frac{2AB}{3} + \frac{B}{\lambda} \right) \tag{40}$$

By the assumption of staggered microcracks, the function ψ_4 is identical to ψ_1 except that it is shifted by half a crack interval:

$$\psi_4 = \begin{cases} \psi_1(\xi - \rho) & \text{for } \xi > 0 \\ \psi_1(\xi + \rho) & \text{for } \xi < 0 \end{cases} \tag{41}$$

In addition to this condition, ψ_1 and all its even derivatives are even, while all its odd derivatives are odd. By virtue of Eq. (41), ψ_1 and ψ_4 are dependent functions, but we can treat them as independent functions if we consider only the interval $(0, \frac{\rho}{2})$ and impose appropriate boundary conditions at $\xi = \frac{\rho}{2}$. After solving for these two independent functions on the interval $(0, \frac{\rho}{2})$, we can construct the complete ψ_1 and ψ_4 functions by symmetry and Eq. (41).

The next step is to reduce the integral for $\Gamma - \Gamma_0$ to an integral on the interval $(0, \frac{\rho}{2})$. The integrand is an even function about $\xi = 0$ and we simply reduce the integral to an integral from 0 to ρ by multiplying by 2. On the interval $(0, \rho)$ we can write $\psi_1(\xi) = \psi_4(\rho - \xi)$ and $\psi_4(\xi) = \psi_1(\rho - \xi)$. With this symmetry, the integral from 0 to $\frac{\rho}{2}$ is equal to the integral from $\frac{\rho}{2}$ to ρ. We therefore use an additional facotr of 2 and rewrite $\Gamma - \Gamma_0$ as

$$\begin{aligned} \Gamma - \Gamma_0 = 4t_1^2 \int_0^{\frac{\rho}{2}} \Big(& C_{11}(\psi_1^2 + \psi_4^2) + C_{21}(\psi_1\psi_1'' + \psi_4\psi_4'') + C_{31}(\psi_1''^2 + \psi_4''^2) + C_{41}(\psi_1'^2 + \psi_4'^2) \\ & - \Delta\alpha T(\psi_1 + \psi_4) + C_{12}\psi_1\psi_4 + C_{22}(\psi_1\psi_4'' + \psi_1''\psi_4) + C_{32}\psi_1''\psi_4'' + C_{42}\psi_1'\psi_4' \Big) d\xi \end{aligned} \tag{42}$$

The boundary conditions on the interval $(0, \frac{\rho}{2})$, which include the symmetry imposed boundary conditions at $\xi = \frac{\rho}{2}$, are

$$\psi_1(0) = \sigma \tag{43}$$

$$\psi_1'(0) = 0 \tag{44}$$

$$\psi_4(0) = \sigma_{x0}^{(1)} \tag{45}$$

$$\psi_4'(0) = 0 \tag{46}$$

$$\psi_1(\frac{\rho}{2}) = \psi_4(\frac{\rho}{2}) \tag{47}$$

$$\psi_1'(\frac{\rho}{2}) = -\psi_4'(\frac{\rho}{2}) \tag{48}$$

where σ, being the value of ψ_1 at $\xi = 0$, is an undetermined constant.

The minimization of the functional $\Gamma - \Gamma_0$ is more conveniently found by recasting in terms of two new functions that are the sum and difference of ψ_1 and ψ_4:

$$X = \psi_1 + \psi_4 \tag{49}$$

$$Y = \psi_1 - \psi_4 \tag{50}$$

The complementary energy in terms of X and Y is

$$\Gamma - \Gamma_0 = t_1^2 \int_0^{\frac{\rho}{2}} \Big(C_1 X^2 + C_2 X X'' + C_3 X''^2 + C_4 X'^2 - 4\Delta\alpha T X + C_1^* Y^2 + C_2^* Y Y'' + C_3^* Y''^2 + C_4^* Y'^2 \Big) d\xi \tag{51}$$

where the new constants are

$$C_1 = 2C_{11} + C_{12} = \frac{1}{E_x^{(1)}} + \frac{1}{\lambda E_x^{(2)}} \tag{52}$$

$$C_2 = 2C_{21} + 2C_{22} = -\frac{\nu_{xz}^{(1)}}{3E_x^{(1)}} + \frac{\nu_{xz}^{(2)}}{E_x^{(2)}}\left(1 + \frac{2\lambda}{3}\right) \tag{53}$$

$$C_3 = 2C_{31} + C_{32} = \frac{1}{20E_z^{(1)}} + \frac{\lambda}{60E_z^{(2)}}\left(8\lambda^2 + 20\lambda + 15\right) \tag{54}$$

$$C_4 = 2C_{41} + C_{42} = \frac{1}{3G_{xz}^{(1)}} + \frac{\lambda}{3G_{xz}^{(2)}} \tag{55}$$

$$C_1^* = 2C_{11} - C_{12} = \frac{1}{E_x^{(1)}} + \frac{(1+2\lambda)^2}{\lambda^3 E_x^{(2)}} \tag{56}$$

$$C_2^* = 2C_{21} - 2C_{22} = -\frac{\nu_{xz}^{(1)}}{3E_x^{(1)}} + \frac{\nu_{xz}^{(2)}}{E_x^{(2)}}\left[\frac{(1+2\lambda)(2+\lambda)}{3\lambda}\right] \tag{57}$$

$$C_3^* = 2C_{31} - C_{32} = \frac{1}{20E_z^{(1)}} + \frac{\lambda}{60E_z^{(2)}}\left(2\lambda^2 + 7\lambda + 8\right) \tag{58}$$

$$C_4^* = 2C_{41} - C_{42} = \frac{1}{3G_{xz}^{(1)}} + \frac{1+\lambda+\lambda^2}{3\lambda G_{xz}^{(2)}} \tag{59}$$

C_1 through C_4 are identical to the constants that appear in the analysis of $[90_n/0_m]_s$ laminates with non-staggered microcracks [15]. The complementary constants C_1^* through C_4^* are new. From Eqs. (43)–(48), the boundary conditions for X and Y are

$$X(0) = \sigma + \sigma_{x0}^{(1)} \tag{60}$$

$$X'(0) = 0 \tag{61}$$

$$X'\Big(\frac{\rho}{2}\Big) = 0 \tag{62}$$

$$Y(0) = \sigma - \sigma_{x0}^{(1)} \tag{63}$$

$$Y'(0) = 0 \tag{64}$$

$$Y\Big(\frac{\rho}{2}\Big) = 0 \tag{65}$$

Treating σ as a given, albeit unknown, constant, the minimization of $\Gamma - \Gamma_0$ is a calculus of variations problem having variable end conditions for $X\big(\frac{\rho}{2}\big)$ and for $Y'\big(\frac{\rho}{2}\big)$ [26]. Taking the first variation of $\Gamma - \Gamma_0$ and accounting for the two variable end conditions yields the following equations:

$$\frac{\partial \Phi}{\partial X} - \frac{\partial}{\partial \xi}\left(\frac{\partial \Phi}{\partial X'}\right) + \frac{\partial^2}{\partial \xi^2}\left(\frac{\partial \Phi}{\partial X''}\right) = 0 \tag{66}$$

$$\frac{\partial \Phi}{\partial Y} - \frac{\partial}{\partial \xi}\left(\frac{\partial \Phi}{\partial Y'}\right) + \frac{\partial^2}{\partial \xi^2}\left(\frac{\partial \Phi}{\partial Y''}\right) = 0 \tag{67}$$

$$\frac{\partial \Phi}{\partial X'} - \frac{\partial}{\partial \xi}\left(\frac{\partial \Phi}{\partial X''}\right) = 0 \qquad \text{at } \xi = \frac{\rho}{2} \tag{68}$$

$$\frac{\partial \Phi}{\partial Y''} = 0 \qquad \text{at } \xi = \frac{\rho}{2} \tag{69}$$

where Φ is the integrand in the $\Gamma - \Gamma_0$ expression. The first two equations lead to two Euler equations for X and Y:

$$X^{iv} + pX'' + qX = \frac{2\Delta\alpha T}{C_3} \tag{70}$$

$$Y^{iv} + p^* Y'' + q^* Y = 0 \tag{71}$$

where

$$\begin{aligned} p &= \frac{C_2 - C_4}{C_3} \qquad & p^* &= \frac{C_2^* - C_4^*}{C_3^*} \\ q &= \frac{C_1}{C_3} & q^* &= \frac{C_1^*}{C_3^*} \end{aligned} \tag{72}$$

Eqs. (68) and (69) give two new boundary conditions:

$$X'''\Big(\frac{\rho}{2}\Big) = 0 \tag{73}$$

$$Y''\Big(\frac{\rho}{2}\Big) = 0 \tag{74}$$

The two Euler equations (Eqs. (70) and (71)) and the eight boundary conditions (Eqs. (60)–(65),(73),(74)) are what we have to solve for X and Y.

The two Euler equations are two uncoupled fourth order differential equations each similar to the equations that resulted from the variational analysis of $[0_n/90_m]_s$ laminates. We can extract their general solutions from the results in Hashin [20,21] and in Nairn [15]. The specific solutions depend on the boundary conditions presented in this paper. The details of the solution process are described in the Appendix.

After solving for X and Y, the solution is complete except for determination of the undetermined constant σ, which can be obtained by finding the value of σ that minimizes $\Gamma - \Gamma_0$. To achieve this second minimization we insert the solutions for X and Y back into the expression for $\Gamma - \Gamma_0$ (Eq. (51)). Fortunately we can use the two Euler equations to simplify this task. Multiplying Eq. (70) by $C_3 X$ and integrating from 0 to $\frac{\rho}{2}$ gives

$$\int_0^{\frac{\rho}{2}} \Big(C_1 X^2 + C_2 X X'' + C_3 X''^2 + C_4 X'^2 - 2\Delta\alpha T X \Big) d\xi = C_3 \left(\sigma + \sigma_{x0}^{(1)} \right) X'''(0) \tag{75}$$

Multiplying Eq. (71) by $C_3^* Y$ and integrating from 0 to $\frac{\rho}{2}$ gives

$$\int_0^{\frac{\rho}{2}} \Big(C_1^* Y^2 + C_2^* Y Y'' + C_3^* Y''^2 + C_4^* Y'^2 \Big) d\xi = C_3^* \left(\sigma - \sigma_{x0}^{(1)} \right) Y'''(0) \tag{76}$$

These result in

$$\Gamma - \Gamma_0 = t_1^2 \Big(C_3 \left(\sigma + \sigma_{x0}^{(1)} \right) X'''(0) + C_3^* \left(\sigma - \sigma_{x0}^{(1)} \right) Y'''(0) - 2\Delta\alpha T \langle X \rangle \Big) \tag{77}$$

where the average value notation means

$$\langle f \rangle = \int_0^{\frac{\rho}{2}} f \, d\xi \tag{78}$$

Substituting $\langle X \rangle$, $X'''(0)$ and $Y'''(0)$ derived in the Appendix into Eq. (77) gives

$$\Gamma - \Gamma_0 = t_1^2 \left[C_3 \left(\sigma + \sigma_{x0}^{(1)} - \frac{2\Delta\alpha T}{C_1} \right)^2 \chi\Big(\frac{\rho}{2}\Big) + C_3^* \left(\sigma - \sigma_{x0}^{(1)} \right)^2 \chi^*\Big(\frac{\rho}{2}\Big) + \frac{2\rho\Delta\alpha^2 T^2}{C_1} \right] \tag{79}$$

The functions $\chi\big(\frac{\rho}{2}\big)$ and $\chi^*\big(\frac{\rho}{2}\big)$ are given in the Appendix and found not to depend on σ. We differentiate Eq. (79) with respect to σ to find the value of σ that minimizes $\Gamma - \Gamma_0$. The result is

$$\sigma = \frac{\sigma_{x0}^{(1)} C_3^* \chi^*\big(\frac{\rho}{2}\big) - \left(\sigma_{x0}^{(1)} - \frac{2\Delta\alpha T}{C_1} \right) C_3 \chi\big(\frac{\rho}{2}\big)}{C_3 \chi\big(\frac{\rho}{2}\big) + C_3^* \chi^*\big(\frac{\rho}{2}\big)} \tag{80}$$

THE EFFECT OF STAGGERED MICROCRACKS

The previous section gives a solution that minimizes the total complementary energy in a $[90_m/0_n]_s$ laminate having staggered microcracks. The solution is expressed in terms of the functions X and Y on the interval $(0, \frac{\rho}{2})$ and the constant σ. This information allows us to construct the functions ψ_1 to ψ_4, which define the stress state, on the interval $(-\rho, \rho)$. In this section we use the obtained stress state to evaluate the effect of staggered microcracks on the sample strain energy, longitudinal modulus, and longitudinal thermal expansion coefficient. From the result for strain energy, we deduce the energy release rate for the formation of new microcracks.

For a given thermoelastic stress state the total strain energy is defined by

$$U = \int_V \vec{\sigma} \cdot \mathbf{K}\vec{\sigma} dV \tag{81}$$

This integral is identical to the first term of Eq. (29). We thus find total strain energy by repeating the evaluation of complementary energy but ignoring the thermal term (the second term in Eq. (29)). The total strain energy per unit depth in the unit cell of damage in terms of X and Y is

$$U = U_0 + t_1^2 \int_0^{\frac{\rho}{2}} \Big(C_1 X^2 + C_2 X X'' + C_3 X''^2 + C_4 X'^2 + C_1^* Y^2 + C_2^* Y Y'' + C_3^* Y''^2 + C_4^* Y'^2 \Big) d\xi \tag{82}$$

where

$$U_0 = \left(\frac{\sigma_0^2}{2E_0} \right) 2\rho t_1 B \tag{83}$$

and $B = 2(t_1 + t_2)$ is the total thickness of the laminate. Using Eqs. (75) and (76) we get

$$U = U_0 + t_1^2 \Big(C_3 \left(\sigma + \sigma_{x0}^{(1)} \right) X'''(0) + C_3^* \left(\sigma - \sigma_{x0}^{(1)} \right) Y'''(0) + 2\Delta\alpha T \langle X \rangle \Big) \tag{84}$$

Inserting the expressions of $X'''(0)$, $Y'''(0)$, $\langle X \rangle$ (given in the Appendix) and σ gives

$$U = \left(\frac{\sigma_0^2}{2E_0} + \frac{t_1 \Delta\alpha^2 T^2}{C_1 B} \right) 2\rho t_1 B + \frac{4t_1^2 C_3 \chi\left(\frac{\rho}{2}\right) C_3^* \chi^*\left(\frac{\rho}{2}\right)}{C_3 \chi\left(\frac{\rho}{2}\right) + C_3^* \chi^*\left(\frac{\rho}{2}\right)} \left({\sigma_{x0}^{(1)}}^2 - \frac{\Delta\alpha^2 T^2}{C_1^2} \right) \tag{85}$$

For better analogy with the variational analysis of $[0_n/90_m]_s$ laminates [15,20,21] we define a new function $\chi_a(\rho)$. The subscript "a" stands for cross-ply laminates with antisymmetric or staggered cracks:

$$\chi_a(\rho) = \frac{2\chi\left(\frac{\rho}{2}\right)}{1 + \frac{C_3 \chi\left(\frac{\rho}{2}\right)}{C_3^* \chi^*\left(\frac{\rho}{2}\right)}} \tag{86}$$

The total strain energy in terms of $\chi_a(\rho)$ is

$$U = \left(\frac{\sigma_0^2}{2E_0} + \frac{t_1 \Delta\alpha^2 T^2}{C_1 B} \right) 2\rho t_1 B + 2t_1^2 C_3 \chi_a(\rho) \left({\sigma_{x0}^{(1)}}^2 - \frac{\Delta\alpha^2 T^2}{C_1^2} \right) \tag{87}$$

This result is identical to the $[0_n/90_m]_s$ laminate result [15] except that the new function $\chi_a(\rho)$ replaces the function $\chi(\rho)$.

We next extend our result to a damaged $[90_m/0_n]_s$ laminate having n microcracks in each 90° ply group. Let the resulting n unit cells of damage be characterized by crack spacings ρ_1, ρ_2, …, ρ_n. Note that the

crack spacings can be variable and we do not have to assume a periodic arrangement of cracks. Let the total sample width in the y direction be W. Summing the strain energies for each unit cell and multiplying by the sample width, the total strain energy is

$$U = \left(\frac{\sigma_0^2}{2E_0} + \frac{t_1 \Delta\alpha^2 T^2}{C_1 B}\right) LBW + t_1 C_3 LW \left(\sigma_{x0}^{(1)^2} - \frac{\Delta\alpha^2 T^2}{C_1^2}\right) \frac{\sum_{i=1}^{n} \chi_a(\rho_i)}{\sum_{i=1}^{n} \rho_i} \tag{88}$$

We use Eq. (88) to evaluate the effective sample modulus — E. In the absence of thermal stresses ($T = 0$), the strain energy and the complementary energy will be equal. By definition, the complementary energy of the damaged laminate in terms of an effective sample modulus, E, is

$$U = \left(\frac{\sigma_0^2}{2E}\right) LBW \tag{89}$$

By the principles of variational mechanics, Eq. (88) gives an upper bound to the true complementary energy in Eq. (89). We thus must have

$$\left(\frac{\sigma_0^2}{2E}\right) LBW \leq \left(\frac{\sigma_0^2}{2E_0}\right) LBW + t_1 C_3 LW \sigma_{x0}^{(1)^2} \frac{\sum_{i=1}^{n} \chi_a(\rho_i)}{\sum_{i=1}^{n} \rho_i} \tag{90}$$

Simplifying Eq. (90) results in

$$\frac{1}{E} \leq \frac{1}{E_0} + \frac{2t_1 C_3 E_x^{(1)^2}}{BE_0^2} \frac{\sum_{i=1}^{n} \chi_a(\rho_i)}{\sum_{i=1}^{n} \rho_i} \tag{91}$$

Multiplying both sides of Eq. (91) by $\frac{L}{BW}$ gives an expression for compliance:

$$C \leq C_0 + \frac{2t_1 C_3 L E_x^{(1)^2}}{B^2 W E_0^2} \frac{\sum_{i=1}^{n} \chi_a(\rho_i)}{\sum_{i=1}^{n} \rho_i} \tag{92}$$

where

$$C_0 = \frac{L}{BE_0 W} \tag{93}$$

is the compliance of the undamaged sample. Although Eq. (91) formally only defines a lower bound to the modulus, the results for $[0_n/90_m]_s$ laminates suggest that it is a tight bound [20]. We therefore expect that Eqs. (91) and (92) also provide a tight bounds to the modulus and compliance of $[90_m/0_n]_s$ laminates with staggered microcracks.

It is useful to rewrite the sample strain energy in terms of sample compliance which is an easily measurable quantity. We solve Eq. (92) for the summation terms involving $\chi_a(\rho_i)$ and ρ_i. Substituting this result into Eq. (88) gives

$$U = \left(\frac{\sigma_0^2}{2E_0} + \frac{t_1 \Delta\alpha^2 T^2}{C_1 B}\right) LBW + (C - C_0) \frac{B^2 W^2 E_0^2}{2E_x^{(1)^2}} \left[\sigma_{x0}^{(1)^2} - \frac{\Delta\alpha^2 T^2}{C_1^2}\right] \tag{94}$$

This expression for strain energy of $[90_m/0_n]_s$ laminates is symbolically identical to the one for $[0_n/90_m]_s$ laminates [15]. Differences in strain energy levels as a function of damage arise due to the different functional forms of the compliance expressions required for use in Eq. (94).

Complete knowledge of the stress state in $[90_m/0_n]_s$ laminates allows us to calculate the effect of temperature on sample displacements. This calculation can be used to predict the longitudinal thermal

expansion coefficient. We begin the calculation by finding the total displacement of the intact 0° plies — layers 2 and 3. The unit cell displacement under load P, $u(P)$, can be found by integrating the strain:

$$u(P) = t_1 \int_{-\rho}^{\rho} \left(\frac{\sigma_{xx}^{(i)}}{E_x^{(i)}} - \frac{\nu_{xz}^{(i)} \sigma_{zz}^{(i)}}{E_x^{(i)}} + \alpha_x^{(i)} T \right) d\xi \tag{95}$$

Using this formula on layers 2 and 3 reveals their displacements to be different. When many crack intervals are included, the appropriate total displacement is the average of the displacements from these two layers. We note the $\sigma_{zz}^{(i)}$ depends only on ψ_1'' and ψ_4''. Because

$$\int_{-\rho}^{\rho} \psi_i'' d\xi = 0 \qquad (\text{for } i = 1 \text{ or } 4) \tag{96}$$

the second term in the displacement equation is zero. Considering only the first and third terms and averaging the results for layers 2 and 3 give

$$u(P) = \frac{1}{2}\big(u_2(P) + u_3(P)\big) = \frac{2\rho t_1 P}{BE_0 W} + 2\rho t_1 \alpha_x^{(2)} T + \frac{2t_1}{\lambda E_x^{(2)}} \langle X \rangle \, d\xi \tag{97}$$

Substituting the expression for $\langle X \rangle$ (given in the Appendix), the average displacement is

$$u(P) = \frac{2\rho t_1 P}{BE_0 W} + 2\rho t_1 \alpha_x^{(2)} T + \frac{t_1 C_3}{\lambda E_x^{(2)} C_1} \left(2\sigma_{x0}^{(1)} - \frac{2\Delta\alpha T}{C_1} \right) \chi_a(\rho) + \frac{2\rho t_1 \Delta\alpha T}{\lambda E_x^{(2)} C_1} \tag{98}$$

Summing over n unit cells of damage yields

$$u(P) = \frac{PL}{BE_0 W} + \alpha_x^{(2)} LT + \frac{L\Delta\alpha T}{\lambda E_x^{(2)} C_1} + \frac{LC_3}{\lambda E_x^{(2)} C_1} \left(\sigma_{x0}^{(1)} - \frac{\Delta\alpha T}{C_1} \right) \frac{\sum_{i=1}^{n} \chi_a(\rho_i)}{\sum_{i=1}^{n} \rho_i} \tag{99}$$

The longitudinal laminate thermal expansion coefficient is defined by

$$\alpha_{Lc} = \frac{u(0)}{LT} = \alpha_x^{(2)} + \frac{\Delta\alpha}{\lambda E_x^{(2)} C_1} - \frac{\Delta\alpha C_3}{\lambda E_x^{(2)} C_1^2} \frac{\sum_{i=1}^{n} \chi_a(\rho_i)}{\sum_{i=1}^{n} \rho_i} \tag{100}$$

The first two terms combine to give

$$\alpha_x^{(2)} + \frac{\Delta\alpha}{\lambda E_x^{(2)} C_1} = 2\frac{t_1 \alpha_x^{(1)} E_x^{(1)} + t_2 \alpha_x^{(2)} E_x^{(2)}}{BE_0} = \alpha_{Lc}^0 \tag{101}$$

which is the longitudinal thermal expansion coefficient of the undamaged laminate. In deriving Eq. (101) we used the rule-of-mixtures sample modulus

$$E_0 = \frac{E_x^{(1)} + \lambda E_x^{(2)}}{1 + \lambda} \tag{102}$$

to rewrite C_1 as

$$C_1 = \frac{BE_0}{2t_2 E_x^{(2)} E_x^{(1)}} \tag{103}$$

As with the sample strain energy, the summation part of the last term in Eq. (100) can be written in terms of the compliance. The final expression for the thermal expansion coefficient becomes

$$\alpha_{Lc} = \alpha_{Lc}^0 - \frac{C - C_0}{C_0} \frac{\Delta\alpha}{C_1 E_T} \tag{104}$$

Eq. (104) is identical to the result for $[0_n/90_m]_s$ laminates [15,24] except of course that the expression for C differs from the C expression for $[0_n/90_m]_s$ laminates

When written in terms of sample compliance, the expressions for sample strain energy and thermal expansion coefficient of a damaged $[90_m/0_n]_s$ laminate are symbolically identical to the corresponding expressions for $[0_n/90_m]_s$ laminates. Any calculation that depends only on these expressions will symbolically be the same for $[0_n/90_m]_s$ and $[90_m/0_n]_s$ laminates. One such calculation is the total energy released due to the formation of new microcracks [15,24]. The total energy release rate on going from one state of microcracking damage to another is found by differentiating the total strain energy (Eq. (94)) at constant displacement

$$G_m = -\frac{\partial U}{\partial A}\Big|_{const.u} = \frac{B^2W^2E_0^2}{2{E_x^{(1)}}^2}\left(\frac{E_x^{(1)}}{E_0}\sigma_0 - \frac{\Delta\alpha T}{C_1}\right)^2\frac{dC}{dA} \tag{105}$$

where A is the total microcrack fracture area ($A = 2t_1nW$). In deriving Eq. (105) we needed to evaluate $\frac{\partial\sigma_0}{\partial A}\big|_{const.\ u}$. Using the relation

$$CP = u(P) - u(0) = u(P) - \alpha_L LT \tag{106}$$

where $P = \sigma_0 BW$ and differentiating result in

$$\frac{\partial\sigma_0}{\partial A}\big|_{const.\ u} = \left(\frac{E_0\Delta\alpha T}{E_x^{(1)}C_1} - \sigma_0\right)\frac{1}{C}\frac{dC}{dA} \tag{107}$$

Evaluating $\frac{dC}{dA}$ by differentiating Eq. (92) and substituting into Eq. (105) result in the final energy release rate expression:

$$G_m = \left(\frac{E_x^{(1)}}{E_0}\sigma_0 - \frac{\Delta\alpha T}{C_1}\right)^2 C_3 t_1 Y(D) \tag{108}$$

where $Y(D)$ is a calibration function that depends on the crack density, $D = \frac{n}{L}$, or more formally on the complete distribution of crack spacings:

$$Y(D) = LW\frac{d}{dA}\frac{\sum_{i=1}^{n}\chi_a(\rho_i)}{\sum_{i=1}^{n}\rho_i} = \frac{d}{dD}\left(D\left\langle\chi_a(\rho)\right\rangle\right) \tag{109}$$

where $\langle\chi_a(\rho)\rangle$ is the average value of $\chi_a(\rho)$ over the n unit cells of damage.

To use Eq. (108), we must evaluate $Y(D)$. As was done for $[0_n/90_m]_s$ laminates [15,24] we evaluate $Y(D)$ by considering a specific fracture event resulting in new microcracks in the k^{th} unit cell of damage. The tendency towards staggered microcracks requires that the new microcracks form in layer 1 at $\xi = \pm\rho/3$ and form in layer 4 at $\xi = \pm 2\rho/3$. As shown in Fig. 3B, these locations for new microcracks divide the existing unit cell of damage into three unit cells of damage, each $\frac{1}{3}$ as large as the original. In the next section we explain why it is reasonable for the new microcracks to form at these specific locations. Before the new microcracks form there are n unit cells of damage and

$$\langle\chi_a(\rho)\rangle = \frac{1}{n}\sum_{i=1}^{n}\chi_a(\rho_i) \qquad \text{and} \qquad D = \frac{n}{L} \tag{110}$$

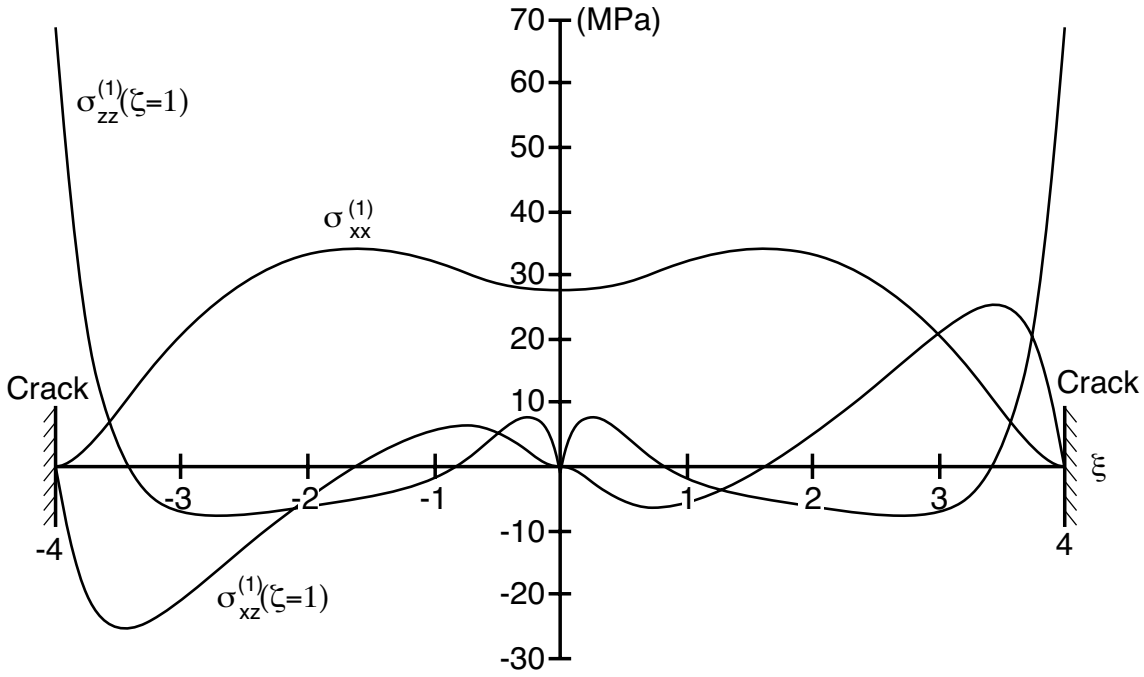

Figure 4: Stresses between two microcracks in the 90° ply group of a Hercules AS4/3501-6 $[90_2/0]_s$ laminate. The applied stress in 100 MPa, the thermal load is $T = -125°$C, and the crack spacing is $\rho = 4$. The normal stress ($\sigma_{xx}^{(1)}$) is for the entire ply group. The plotted shear stress ($\sigma_{xz}^{(1)}$) and transverse stress ($\sigma_{zz}^{(1)}$) are the stresses at the interface between the 90° and 0° ply group.

After the new microcracks form in the k^{th} unit cell of damage there will be $n+2$ unit cells of damage and

$$\langle \chi_a(\rho) \rangle = \frac{1}{n+2} \left[\left(\sum_{i=1}^{n} \chi_a(\rho_i) \right) - \chi_a(\rho_k) + 3\chi_a(\rho_k/3) \right] \qquad \text{and} \qquad D = \frac{n+2}{L} \tag{111}$$

By a discrete evaluation of the derivative in Eq. (109) the calibration function is

$$Y(D) = \frac{\Delta\big(D\,\langle \chi_a(\rho) \rangle\big)}{\Delta D} = \frac{1}{2}\big(3\chi_a(\rho_k/3) - \chi_a(\rho_k)\big) \tag{112}$$

For relatively uniform crack spacings, ρ_k can be replaced by the average value or ρ_i or $\rho = \frac{1}{2t_1 D}$. The final expression for the energy release rate is

$$G_m = \frac{1}{2} \left(\frac{E_x^{(1)}}{E_0} \sigma_0 - \frac{\Delta\alpha T}{C_1} \right)^2 C_3 t_1 \big(3\chi_a(\rho/3) - \chi_a(\rho)\big) \tag{113}$$

RESULTS

In this section we plot the results of the previous section for a specific example of a $[90_2/0]_s$ Hercules 3501-6/AS4 laminate. We assume the following mechanical properties

$$E_x^{(1)} = E_z^{(1)} = E_z^{(2)} = 9700 \text{ MPa} \qquad G_{xz}^{(2)} = 5000 \text{ MPa} \qquad \alpha_x^{(1)} = \alpha_z^{(1)} = \alpha_z^{(2)} = 28.8\ 10^{-6}\ {}^\circ C^{-1}$$
$$E_x^{(2)} = 130000 \text{ MPa} \qquad \nu_{xz}^{(1)} = 0.5 \qquad \alpha_x^{(2)} = -0.09\ 10^{-6}\ {}^\circ C^{-1}$$
$$G_{xz}^{(1)} = 3600 \text{ MPa} \qquad \nu_{xz}^{(2)} = 0.3 \qquad 0.154 \text{ mm per ply}$$

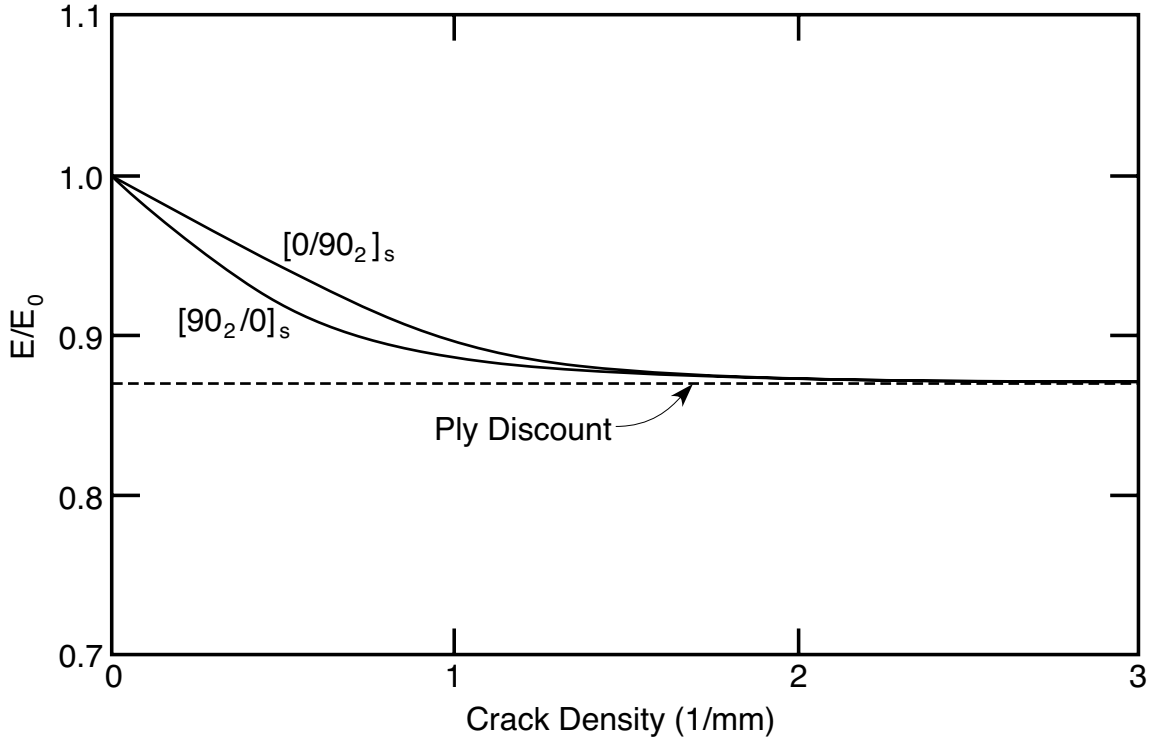

Figure 5: The ratio of the modulus of a damaged Hercules AS4/3501-6 laminate to the modulus of an undamaged laminate as a function of crack density. The two plots compare the results for a $[90_2/0]_s$ laminate and a $[0/90_2]_s$ laminate. The dashed line is the modulus for a laminate with discounted 90° plies.

The stresses in the 90° ply group on the left edge of the laminate in Fig. 3A, or the stresses between two existing microcracks are plotted in Fig. 4. The stresses are calculated for a specific applied stress of $\sigma_0 = 100$ MPa, a thermal load caused by a temperature differential of $T = -125°$C, and a unit cell of damage characterized by $\rho = 4$. The tensile stress ($\sigma_{xx}^{(1)}$) is zero at the two crack faces as required by boundary conditions. Midway between the two microcracks and directly opposite the crack in the 90° ply group on the opposing surface (see Fig. 3A) there is a local minimum in tensile stress. This local minimum is caused by a bending effect that results from the asymmetric nature of the unit cell of damage. Two local maxima in tensile stress are located at positions close to $\frac{1}{3}$ and $\frac{2}{3}$ of the way from the bottom microcrack to the top microcrack. The form of the tensile stresses shown in Fig. 4 can be used to explain the tendency towards staggered microcracks. Figure 3B shows a unit cell of damage with new microcracks formed at all local tensile stress maxima. The new damage state is equivalent to three unit cells of damage each $\frac{1}{3}$ as large as the initial unit cell of damage. Thus forming microcracks at maxima in tensile stresses leads to propagation of staggered microcracks. For microcracks that are farther apart (ρ gets larger), the local stress maxima are less pronounced. This result suggests that the tendency towards staggered microcracks will be weak when there are few microcracks but become stronger as the crack density increases.

The shear stress ($\sigma_{xz}^{(1)}(\zeta = 1)$) plotted in Fig. 4 is the shear stress at the interface between the 90° and 0° ply groups. As required by boundary conditions, the shear stress is zero on the crack faces. The shear stress is also zero at $\xi = 0$; this zero shear stress is a consequence of symmetry. The peak shear stress is

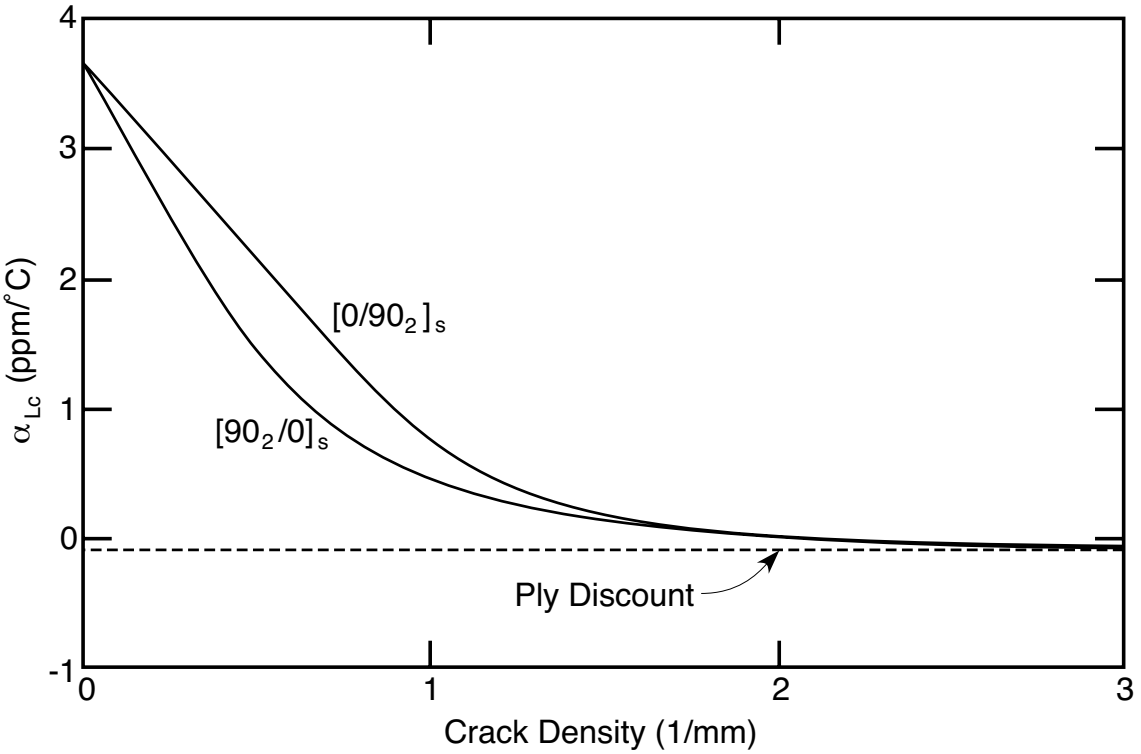

Figure 6: The longitudinal thermal expansion coefficient of a Hercules AS4/3501-6 laminate as a function of crack density. The two plots compare the results for a $[90_2/0]_s$ laminate and a $[0/90_2]_s$ laminate. The dashed line is the longitudinal thermal expansion coefficient of the 0° plies.

similar in magnitude, but less than the peak tensile stress.

The transverse stress ($\sigma_{zz}^{(1)}(\zeta = 1)$) plotted in Fig. 4 is the transverse stress at the interface between the 90° and 0° ply groups. There is a significant transverse stress concentration at the microcrack tip. The peak transverse stress is tensile and about twice as large as the peak $\sigma_{xx}^{(1)}$ stress. In dramatic contrast, the corresponding interfacial transverse stress in $[0/90_2]_s$ laminates shows a compressive stress concentration near the microcrack tips [20]. The difference between $[90_2/0]_s$ and $[0/90_2]_s$ laminates is the bending effect caused by the asymmetric unit cell in $[90_2/0]_s$ laminates. The same bending effect that caused the local minimum in $\sigma_{xx}^{(1)}$ causes the interfacial transverse tensile stress near the microcrack tips. This high tensile transverse stress can be expected to promote mode I delamination initiating from the tips of microcracks. The differences in transverse tensile stresses between $[90_2/0]_s$ and $[0/90_2]_s$ laminates suggest that delamination failure will be more likely in $[90_2/0]_s$ laminates than in $[0/90_2]_s$ laminates. This suggestion agrees with preliminary observations [14].

In Figs. 5 and 6 we plot the effect of microcracks on the mechanical properties of cross-ply laminates as a function of crack density. Each plot gives the results for a $[90_2/0]_s$ laminate and gives a comparison to a $[0/90_2]_s$ laminate. Also shown in each plot is a dashed line labeled "Ply Discount." The dashed line is the result for a laminate in which the 90° plies are discounted and assumed to have zero modulus. The results for both laminates should, and do, asymptotically approach this dashed line in the limit of large crack density. In these two figures we note that both the laminate longitudinal modulus and the laminate longitudinal

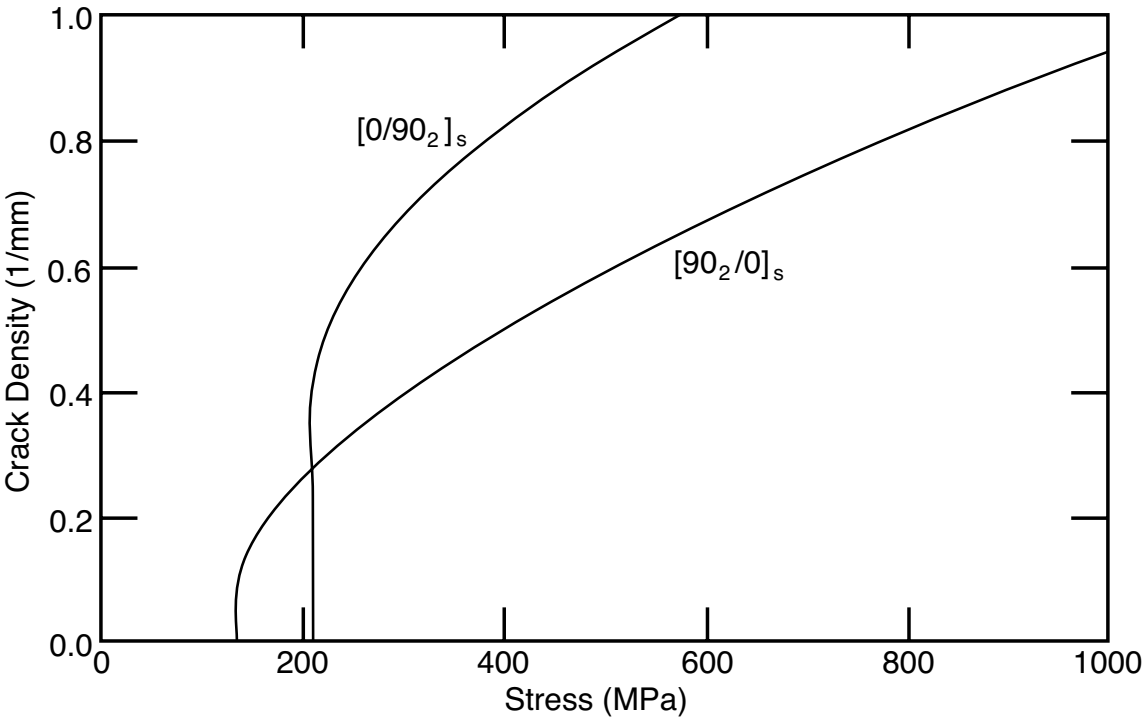

Figure 7: The crack density in a Hercules AS4/3501-6 laminate as a function of applied stress. The two plots compare the results for a $[90_2/0]_s$ laminate and a $[0/90_2]_s$ laminate.

thermal expansion coefficient degrade more rapidly in $[90_2/0]_s$ laminates than in $[0/90_2]_s$ laminates. Thus at moderate levels of microcracking damage, or at levels commonly observed in real laminates [24], microcracks in $[90_m/0_n]_s$ laminates will cause a larger reduction in properties than microcracks in $[0_n/90_m]_s$ laminates.

In Fig. 7 we plot a fracture mechanics prediction of the crack density as a function of applied stress during static loading. The fracture mechanics prediction is made by assuming that the next microcrack will form when the energy released upon forming that microcrack is greater than or equal to some critical energy release rate—G_{mc}. G_{mc} has a physical interpretation as the microcracking fracture toughness or the *intralaminar* fracture toughness. If G_{mc} is known, it can be equated to G_m in Eq. (113)and solved for σ_0 to give the stress required to form the next microcrack for a given laminate structure and current crack density. Inverting this result gives a prediction of the crack density as a function of applied stress. The result of this calculation is plotted in Fig. 7. The corresponding result for the $[0/90_2]_s$ laminate uses the energy release rate analysis in Nairn [15] and in Liu and Nairn [24].

The fracture mechanics prediction of microcrack density requires knowledge of G_{mc}. This toughness property has been measured for Hercules 3501-6/AS4 laminates using static tests on $[0_m/90_n]_s$ laminates. The measured toughness was found to be $G_{mc} = 240$ J/m^2 [24]; this measured toughness was used to generate the predictions in Fig. 7. The prediction is that microcracks will begin to form in $[90_2/0]_s$ laminates before they begin in $[0/90_2]_s$ laminates. At high loads, the $[0/90_2]_s$ laminate will reach a higher crack density than the $[90_2/0]_s$ laminate. Both of these predictions are in agreement with experimental observations [3,13,14].

DISCUSSION AND CONCLUSIONS

The analyses of microcracking in both $[90_m/0_n]_s$ and $[0_n/90_m]_s$ laminates requires two distinct solutions. The major factor preventing a single analysis is that the microcracks in $[90_m/0_n]_s$ laminates are staggered or antisymmetric while the microcracks in $[0_n/90_m]_s$ laminates are symmetric. The effect of the different damage states can only be assessed by using an analysis technique that is affected by the crack pattern. One such analysis technique is the variational mechanics approach originally developed by Hashin [20,21]. The major result of this paper is an extension of the variational mechanics approach to account for staggered microcracks. The new analysis is considerably more complex but can be cast in a form analogous to the analysis of $[0_n/90_m]_s$ laminates.

Predictions of the new analysis of $[90_m/0_n]_s$ laminates have been compared to the predictions of the corresponding analysis of $[0_n/90_m]_s$ laminates. The different laminate structures and damage states cause differences in the effect that microcracks have on laminate mechanical properties. In particular, both the laminate longitudinal modulus and the laminate longitudinal thermal expansion coefficient decrease more rapidly as a function of damage in $[90_m/0_n]_s$ laminates than they do in $[0_n/90_m]_s$ laminates. The effect on mechanical properties are relatively minor, however, when compared to the effect on failure properties. Microcracks initiate at a lower applied stress in $[90_m/0_n]_s$ laminates, but fail to develop to an extent of microcracking damage that is observed for $[0_n/90_m]_s$ laminates. The transverse normal stress at the interface between the 90° and 0° ply groups is large and tensile in $[90_m/0_n]_s$, a result that is in marked contrast to the corresponding stress in $[0_n/90_m]_s$ laminates which is smaller and compressive. The transverse tensile stress renders $[90_m/0_n]_s$ laminates more susceptible to microcrack induced mode I delaminations.

Some of the differences between $[90_m/0_n]_s$ laminates and $[0_n/90_m]_s$ laminates can be understood by considering bending effects. $[0_n/90_m]_s$ laminates are symmetric and bending effects make no contribution to the analysis. The unit cell of damage in $[90_m/0_n]_s$ laminates, however, is not symmetric and the asymmetry leads to a net bending moment. That bending moment causes the unit cell of damage to curve towards the intact 90° ply group and away from the 90° ply group that has a microcrack at $\xi = 0$ (see Fig. 3A where curving is towards the left). Such a bending effect will create compression at $\xi = 0$ in the intact 90° ply group. This compression effect superposed on the net tensile load causes a the local minimum in $\sigma_{xx}^{(1)}$ plotted in Fig. 4. The bending effect will also create tensile effects at $\xi = 0$ in the 90° ply group that has a microcrack at $\xi = 0$. The tensile effect is to pull the 90° ply group away from the 0° ply group. The pulling effect is manifested by a large tensile transverse stress at the interface between to 90° and 0° ply groups (see Fig. 4).

In summary, there are three major predictions that distinguish the failure properties of $[90_m/0_n]_s$ laminates from those of $[0_n/90_m]_s$ laminates:

1. The load to initiate microcracks is significantly lower for $[90_m/0_n]_s$ laminates.
2. On continued loading, $[90_m/0_n]_s$ laminates develop fewer microcracks. This prediction manifests itself as a lower saturation crack density in $[90_m/0_n]_s$ laminates than in $[0_n/90_m]_s$ laminates.
3. Net bending effects tend to promote mode I delamination in $[90_m/0_n]_s$ laminates. A similar driving

force for delamination is not found in $[0_n/90_m]_s$ laminates.

All these predictions are in agreement with the few experiment results available in the literature [3,13,14]. We are in the process of conducting new experiments on a variety of $[90_m/0_n]_s$ laminates. These new experiments will be used as a quantitative test of this new analysis.

ACKNOWLEDGEMENTS

This work was supported in part by a contract from NASA Langley Research Center (NAS1-18833) monitored by Dr. John Crews, in part by a gift from ICI Advanced Composites monitored by Dr. J. A. Barnes, and in part by a gift from the Fibers Department of E. I. duPont deNemours & Company monitored by Dr. Alan R. Wedgewood. The authors also thank Dr. Dean C. Nairn for some helpful suggestions leading to the final calculus of variations solution.

REFERENCES

1. H. T. Hahn and S. W. Tsai, On the Behavior of Composite Laminates After Initial Failures. *J. Comp. Mat.*, **8**, 299 (1974).
2. K. W. Garrett and J. E. Bailey, Multiple Transverse Fracture in 90° Cross-Ply Laminates of a Glass Fibre-Reinforced Polyester. *J. Comp. Mat.*, **12**, 157 (1977).
3. A. L. Highsmith and K. L. Reifsnider, Stiffness-Reduction Mechanisms in Composite Laminates. *ASTM STP*, **775**, 103 (1982).
4. A. Parvizi, K. W. Garrett, and J. E. Bailey, Constrained Cracking in Glass Fiber-Reinforced Epoxy Cross-Ply Laminates. *J. Mat. Sci.*, **13**, 195 (1978).
5. D. L. Flaggs and M. H. Kural, Experimental Determination of the In Situ Transverse Lamina Strength in Graphite/Epoxy Laminates. *J. Comp. Mat.*, **16**, 103 (1982).
6. M. G. Bader, J. E. Bailey, P. T. Curtis, and A. Parvizi, The Mechanisms of Initiation and Development of Damage in Multi-Axial Fibre-Reinforced Plastics Laminates. *Proc.* 3^{rd} *Int'l Conf. on Mechanical Behavior of Materials*, **3**, 227 (1979).
7. J. E. Bailey, P. T. Curtis and A. Parvizi, On the Trans. Cracking and Long. Splitting Behavior of Glass and Carbon Fibre Epoxy X-Ply Laminates and the Effect of Poisson and Thermally Generated Strains. *Proc. R. Soc. Lond. A*, **366**, 599 (1979).
8. S. E. Groves, C. E. Harris, A. L. Highsmith, and R. G. Norvell, An Experimental and Analytical Treatment of Matrix Cracking in Cross-Ply Laminates. *Experimental Mechanics*, **March**, 73 (1987).
9. L. Boniface, P. A. Smith, S. L. Ogin, and M. G. Bader, Observations on Transverse Ply Crack Growth in a $[0/90_2]_s$ CFRP Laminate Under Monotonic and Cyclic Loading. *Proc.* 6^{th} *Int'l Conf. on Composite Materials*, **3**, 156 (1987).
10. L. Boniface and S. L. Ogin, Application of the Paris Equation to the Fatigue Growth of Transverse Ply Cracks. *J. Comp. Mat.*, **23**, 735 (1989).
11. R. G. Spain, Thermal Microcracking of Carbon Fibre/Resin Composites. *Composites*, **2**, 33 (1971).
12. C. T. Herakovich and M. W. Hyer, Damage-Induced Property Changes in Composites Subjected to

Cyclic Thermal Loading. *Eng. Fract. Mech.*, **25**, 779 (1986).

13. W. W. Stinchcomb, K. L. Reifsnider, P. Yeung, and J. Masters, Effect of Ply Constraint on Fatigue Damage Development in Composite Material Laminates. *ASTM STP*, **723**, 64 (1981).
14. J. Bark, S. Hu, and J. A. Nairn, unpublished results (1990).
15. J. A. Nairn, The Strain Energy Release Rate of Composite Microcracking: A Variational Approach. *J. Comp. Mat.*, **23**, 1106 (1989). (A erratum for this paper published as *J. Comp. Mat.*, **24**, 233 (1990)).
16. Z. Hashin, Thermal Expansion Coefficients of Cracked Laminates. *Composites Science and Technology*, **31**, 247 (1988).
17. K. C. Jen and C. T. Sun, Matrix Cracking and Delamination Prediction in Graphite/Epoxy Laminates. *Proc. of the* 5^{th} *Tech. Conf. of the Amer. Soc. of Composites*, 350 (1990).
18. P. W. Manders, T. W. Chou, F. R. Jones, and J. W. Rock, Statistical Analysis of Multiple Fracture in [0/90/0] Glass Fiber/Epoxy Resin Laminates. *J. Mat. Sci.*, **19**, 2876 (1983).
19. D. L. Flaggs, Prediction of Tensile Matrix Failure in Composite Laminates. *J. Comp. Mat.*, **19**, 29 (1985).
20. Z. Hashin, Analysis of Cracked Laminates: A Variational Approach. *Mechanics of Materials*, **4**, 121 (1985).
21. Z. Hashin, Analysis of Stiffness Reduction of Cracked Cross-Ply Laminates. *Eng. Fract. Mech.*, **25**, 771 (1986).
22. Z. Hashin, Analysis of Orthogonally Cracked Laminates Under Tension. *J. Appl. Mech.*, **54**, 872 (1987).
23. S. Liu and J. A. Nairn, Fracture Mechanics Analysis of Composite Microcracking: Experimental Results in Fatigue. *Proc. of the* 5^{th} *Tech. Conf. of the Amer. Soc. of Composites*, 287 (1990).
24. S. Liu and J. A. Nairn, The Formation and Propagation of Matrix Microcracks in Cross-Ply Laminates During Static Loading. *J. Comp. Mat.*, submitted (1990).
25. D. E. Carlson, Linear Thermoelasticity. In *Mechanics of Solids: Volume II*, ed. C. Truesdell, Springer-Verlag, Berlin, p325 (1984).
26. C. Fox, *The Calculus of Variations*, Dover Publications, New York (1987).

APPENDIX

In this appendix we solve for X and Y. There are two cases to consider for each function. When $\frac{p^2}{4} - q < 0$ the solution for X is

$$X = A_1 \cosh\alpha\xi \cos\beta\xi + A_2 \sinh\alpha\xi \sin\beta\xi + A_3 \sinh\alpha\xi \cos\beta\xi + A_4 \cosh\alpha\xi \sin\beta\xi + \frac{2\Delta\alpha T}{C_1} \qquad (A-1)$$

where

$$\alpha = \frac{1}{2}\sqrt{2\sqrt{q} - p} \qquad (A-2)$$

$$\beta = \frac{1}{2}\sqrt{2\sqrt{q} + p} \qquad (A-3)$$

When $\frac{p^2}{4} - q > 0$ the solution for X is

$$X = A_1 \cosh\alpha\xi + A_2 \cosh\beta\xi + A_3 \sinh\alpha\xi + A_4 \sinh\beta\xi + \frac{2\Delta\alpha T}{C_1} \qquad (A-4)$$

where

$$\alpha = \sqrt{-\frac{p}{2} + \sqrt{\frac{p^2}{4} - q}} \tag{A-5}$$

$$\beta = \sqrt{-\frac{p}{2} - \sqrt{\frac{p^2}{4} - q}} \tag{A-6}$$

The general solutions for Y are similar except that they do not have the constant particular solution term. When $\frac{p^{*2}}{4} - q^* < 0$ the solution for Y is

$$Y = B_1 \cosh \alpha^* \xi \cos \beta^* \xi + B_2 \sinh \alpha^* \xi \sin \beta^* \xi + B_3 \sinh \alpha^* \xi \cos \beta^* \xi + B_4 \cosh \alpha^* \xi \sin \beta^* \xi \tag{A-7}$$

where

$$\alpha^* = \frac{1}{2}\sqrt{2\sqrt{q^*} - p^*} \tag{A-8}$$

$$\beta^* = \frac{1}{2}\sqrt{2\sqrt{q^*} + p^*} \tag{A-9}$$

When $\frac{p^{*2}}{4} - q^* > 0$ the solution for Y is

$$Y = B_1 \cosh \alpha^* \xi + B_2 \cosh \beta^* \xi + B_3 \sinh \alpha^* \xi + B_4 \sinh \beta^* \xi \tag{A-10}$$

where

$$\alpha^* = \sqrt{-\frac{p^*}{2} + \sqrt{\frac{p^{*2}}{4} - q^*}} \tag{A-11}$$

$$\beta^* = \sqrt{-\frac{p^*}{2} - \sqrt{\frac{p^{*2}}{4} - q^*}} \tag{A-12}$$

There are eight unknowns — A_1 to A_4 and B_1 to B_4. To find these unknowns we have eight boundary conditions (Eqs. (60)–(65),(73),(74)). Solving the two seperable systems of four linear equations yields the dersired results. When $\frac{p^2}{4} - q < 0$

$$A_1 = \left(\sigma + \sigma_{x0}^{(1)} - \frac{2\Delta\alpha T}{C_1}\right) \tag{A-13}$$

$$A_2 = -\left(\sigma + \sigma_{x0}^{(1)} - \frac{2\Delta\alpha T}{C_1}\right) \frac{\alpha \sinh \alpha\rho - \beta \sin \beta\rho}{\beta \sinh \alpha\rho + \alpha \sin \beta\rho} \tag{A-14}$$

$$A_3 = -\left(\sigma + \sigma_{x0}^{(1)} - \frac{2\Delta\alpha T}{C_1}\right) \frac{\beta(\cosh \alpha\rho - \cos \beta\rho)}{\beta \sinh \alpha\rho + \alpha \sin \beta\rho} \tag{A-15}$$

$$A_4 = \left(\sigma + \sigma_{x0}^{(1)} - \frac{2\Delta\alpha T}{C_1}\right) \frac{\alpha(\cosh \alpha\rho - \cos \beta\rho)}{\beta \sinh \alpha\rho + \alpha \sin \beta\rho} \tag{A-16}$$

When $\frac{p^2}{4} - q > 0$

$$A_1 = \left(\sigma + \sigma_{x0}^{(1)} - \frac{2\Delta\alpha T}{C_1}\right) \frac{\beta \tanh \frac{\beta\rho}{2}}{\beta \tanh \frac{\beta\rho}{2} - \alpha \tanh \frac{\alpha\rho}{2}} \tag{A-17}$$

$$A_2 = -\left(\sigma + \sigma_{x0}^{(1)} - \frac{2\Delta\alpha T}{C_1}\right) \frac{\alpha \tanh \frac{\alpha\rho}{2}}{\beta \tanh \frac{\beta\rho}{2} - \alpha \tanh \frac{\alpha\rho}{2}} \tag{A-18}$$

$$A_3 = -\left(\sigma + \sigma_{x0}^{(1)} - \frac{2\Delta\alpha T}{C_1}\right) \frac{\beta \tanh \frac{\alpha\rho}{2} \tanh \frac{\beta\rho}{2}}{\beta \tanh \frac{\beta\rho}{2} - \alpha \tanh \frac{\alpha\rho}{2}} \tag{A-19}$$

$$A_4 = \left(\sigma + \sigma_{x0}^{(1)} - \frac{2\Delta\alpha T}{C_1}\right) \frac{\alpha \tanh \frac{\alpha\rho}{2} \tanh \frac{\beta\rho}{2}}{\beta \tanh \frac{\beta\rho}{2} - \alpha \tanh \frac{\alpha\rho}{2}} \tag{A-20}$$

When $\frac{p^{*2}}{4} - q^* < 0$

$$B_1 = \left(\sigma - \sigma_{x0}^{(1)}\right) \tag{A-21}$$

$$B_2 = -\left(\sigma - \sigma_{x0}^{(1)}\right) \frac{\alpha^* \sinh \alpha^* \rho + \beta^* \sin \beta^* \rho}{\beta^* \sinh \alpha^* \rho - \alpha^* \sin \beta^* \rho} \tag{A-22}$$

$$B_3 = -\left(\sigma - \sigma_{x0}^{(1)}\right) \frac{\beta^* \left(\cosh \alpha^* \rho + \cos \beta^* \rho\right)}{\beta^* \sinh \alpha^* \rho - \alpha^* \sin \beta^* \rho} \tag{A-23}$$

$$B_4 = \left(\sigma - \sigma_{x0}^{(1)}\right) \frac{\alpha^* \left(\cosh \alpha^* \rho + \cos \beta^* \rho\right)}{\beta^* \sinh \alpha^* \rho - \alpha^* \sin \beta^* \rho} \tag{A-24}$$

When $\frac{p^{*2}}{4} - q^* > 0$

$$B_1 = \left(\sigma - \sigma_{x0}^{(1)}\right) \frac{\beta^* \tanh \frac{\alpha^* \rho}{2}}{\beta^* \tanh \frac{\alpha^* \rho}{2} - \alpha^* \tanh \frac{\beta^* \rho}{2}} \tag{A-25}$$

$$B_2 = -\left(\sigma - \sigma_{x0}^{(1)}\right) \frac{\alpha^* \tanh \frac{\beta^* \rho}{2}}{\beta^* \tanh \frac{\alpha^* \rho}{2} - \alpha^* \tanh \frac{\beta^* \rho}{2}} \tag{A-26}$$

$$B_3 = -\left(\sigma - \sigma_{x0}^{(1)}\right) \frac{\beta^*}{\beta^* \tanh \frac{\alpha^* \rho}{2} - \alpha^* \tanh \frac{\beta^* \rho}{2}} \tag{A-27}$$

$$B_4 = \left(\sigma - \sigma_{x0}^{(1)}\right) \frac{\alpha^*}{\beta^* \tanh \frac{\alpha^* \rho}{2} - \alpha^* \tanh \frac{\beta^* \rho}{2}} \tag{A-28}$$

In the text of the paper we write $\Gamma - \Gamma_0$ and the strain energy U in terms of the $\langle X \rangle$, $X'''(0)$, and $Y'''(0)$. In the remainder of this appendix we evaluate these terms for the above solutions for X and Y. Integrating X form 0 to $\frac{\rho}{2}$ gives after much trigonometric simplification

$$\langle X \rangle = \left(\sigma + \sigma_{x0}^{(1)} - \frac{2\Delta\alpha T}{C_1}\right) \frac{C_3}{C_1} \chi\left(\frac{\rho}{2}\right) + \frac{\rho \Delta \alpha T}{C_1} \tag{A-29}$$

The $\chi(\rho)$ function is

$$\chi(\rho) = 2\alpha\beta\left(\alpha^2 + \beta^2\right) \frac{\cosh 2\alpha\rho - \cos 2\beta\rho}{\beta \sinh 2\alpha\rho + \alpha \sin 2\beta\rho} \tag{A-30}$$

when $\frac{p^2}{4} - q < 0$ and is

$$\chi(\rho) = \alpha\beta\left(\beta^2 - \alpha^2\right) \frac{\tanh \alpha\rho \tanh \beta\rho}{\beta \tanh \beta\rho - \alpha \tanh \alpha\rho} \tag{A-31}$$

When $\frac{p^2}{4} - q > 0$. The $\chi(\rho)$ function in Eq. (A-30) is identical to the function defined during the variational analysis of $[0_n/90_m]_s$ laminates [15,20,21]. The $\chi(\rho)$ function in Eq. (A-31) is identical to an additional function defined during further variational analysis of $[0_n/90_m]_s$ laminates [15].

We evaluate $X'''(0)$ and $Y'''(0)$ by straightforward differentiation of the general expressions for X and Y. For both $\frac{p^2}{4} - q < 0$ and $\frac{p^2}{4} - q > 0$

$$X'''(0) = \left(\sigma + \sigma_{x0}^{(1)} - \frac{2\Delta\alpha T}{C_1}\right) \chi\left(\frac{\rho}{2}\right) \tag{A-32}$$

where $\chi(\rho)$ is defined by Eq. (A-30) or Eq. (A-31), depending on the sign of $\frac{p^2}{4} - q$. For $Y'''(0)$ we have

$$Y'''(0) = \left(\sigma - \sigma_{x0}^{(1)}\right) \chi^*\left(\frac{\rho}{2}\right) \tag{A-33}$$

where the new function complementary to $\chi(\rho)$ is

$$\chi^*(\rho) = 2\alpha^*\beta^*\left(\alpha^{*2} + \beta^{*2}\right)\frac{\cosh 2\alpha^*\rho + \cos 2\beta^*\rho}{\beta^*\sinh 2\alpha^*\rho - \alpha^*\sin 2\beta^*\rho} \qquad (A-34)$$

when $\frac{p^{*2}}{4} - q^* < 0$ and is

$$\chi^*(\rho) = \alpha^*\beta^*\left(\beta^{*2} - \alpha^{*2}\right)\frac{1}{\beta^*\tanh\alpha^*\rho - \alpha^*\tanh\beta^*\rho} \qquad (A-35)$$

when $\frac{p^{*2}}{4} - q^* > 0$.